

Why do mayflies change their gill kinematics as they grow?

R. Chabreyrie¹, K. Abdelaziz², E. Balaras¹, K. Kiger²

¹Department of Mechanical and Aerospace Engineering,
The George Washington University, USA

²Department of Mechanical Engineering,
University of Maryland, USA

March 22, 2022

Abstract

The mayfly nymph breathes under water through an oscillating array of wing-shaped tracheal gills. As the nymph grows, the kinematics of these gills change abruptly from rowing to flapping. The classical fluid dynamics approach to consider the mayfly nymph as a pumping device fails in giving clear reasons to this switch. In order to understand the whys and the hows of this switch between the two distinct kinematics, we analyze the problem under a Lagrangian viewpoint. We consider that a good Lagrangian transport that distributes and spreads water and dissolved oxygen well between and around the gills is the main goal of the gill motion. Using this Lagrangian approach we are able to provide the reason behind the switch from rowing to flapping that the mayfly nymph experiences as it grows. More precisely, recent and powerful tools from this Lagrangian approach are applied to in-silico mayfly nymph experiments, where body shape, as well as, gill shapes, structures and kinematics are matched to those from in-vivo. In this letter, we show both qualitatively and quantitatively how the change of kinematics enables a better attraction, stirring and confinement of water charged of dissolved oxygen inside the gills area. From the computational velocity field we reveal attracting barriers to

transport, i.e. attracting Lagrangian coherent structures, that form the transport skeleton between and around the gills. In addition, we quantify how well the fluid particles and consequently dissolved oxygen is spread and stirred inside the gills area.

Animals have evolved diverse kinematics to generate flows for locomotion, feeding, cooling and breathing and there seems to be a trend between these kinematic patterns and the scale of such systems, as captured by the Reynolds number ($Re = UL/\nu$, where U and L are characteristic velocity and length scales respectively, and ν the kinematic viscosity of the fluid) Strathmann (1993); Walker (2002). In particular, the basic trends, which are fairly well understood at high and low Re indicate that: rowing (i.e. net flow directed ventrally and mostly parallel to the stroke plane) is exclusively used at $Re < 1$ (see for example Taylor (1951); Gray and Hancock (1955); Lighthill (1976); Brennen and Winet (1997) for flagella and cilia locomotion), whereas flapping (i.e. net flow directed dorsally and essentially transverse to the stroke plane) is predominantly used at $Re > 100$ (see Daniel *et al.* (1992); Motani (2002); Spedding *et al.* (2003) for swimming or flying vertebrates). At the less studied intermediate regime $Re = 1 - 20$, Webb and Weihs (1986); Daniel and Webb (1987); Daniel *et al.* (1992); Fuiman and Batty (1997); Walker (2002); Childress and Dudley (2004), the same rule of thumb seems to be valid, when the primary function is the generation of a propulsive force. Appendage kinematics also serve other purposes than locomotion, such as feeding or breathing, where transport (with the specific goals of attracting, stirring and trapping) maybe more important than generating a propulsive hydrodynamic force. Such systems have received far less attention compared to locomotion, and there is a wealth of interesting phenomena to explore that may bring to fruition new, bio-inspired, sensor designs.

In the present work we will focus on mayflies, which are insects belonging to the order of *Ephemeroptera*, referring to their brief adulthood lifespan of only a few days. Most of a mayfly's lifecycle is spent as a nymph in submerged in wetlands, ponds and river habitats in poorly oxygenated water. The mayfly nymphs breathe through tracheal tubes that transport oxygen directly into the tissue Wigglesworth (1931). In the species considered in this study, these tracheal tubes branch out to a series of seven pairs of wing-shaped protrusions known as tracheal gills (see Fig. 1). Today it is established that these gills play a major role in the metabolic respiration Babák and Foustka (1907).

The water current generated by the motion of these gills was first observed by Eastham (1934, 1936, 1937) in the 30s. It was not until recently, however, that more precise quantitative descriptions were reported, which revealed an interesting feature: as mayfly nymphs grow older they sharply change their gill kinematics from rowing to flapping Sensenig *et al.* (2009). Sensenig *et al.* (2010), conducted detailed quantitative measurements and suggested that the observed switch is determined by the size of the vortex generated at the space between the gills.

Abdelaziz *et al.* (2013) used a realistic mayfly model (see Fig. 1a) and prescribed the gill kinematics reported in Sensenig *et al.* (2010) (see Fig. 1d-g), to conduct full Navier-Stokes simulations for a range of Reynolds numbers. They demonstrated that if the mayfly is viewed as a pumping device, then the resulting mechanical efficiency (i.e. the equivalent to the mechanical efficiency of a hydraulic pump, which can be derived from the mechanical energy conservation) is always better for rowing kinematics at any Reynolds number. They also examined another pumping performance parameter, defined as the ratio of the time averaged mass flow rate towards the mayfly to the time averaged rate of work done by the gills, which indicated a slight superiority of flapping kinematics at higher Reynolds numbers. In this letter, we will consider a Lagrangian viewpoint, which follows fluid particles as they proceed in time, to study the breathing mechanism and its relation to the sharp change in the kinematic patterns. Our basic hypothesis is that efficient transport, which attracts and stirs the Lagrangian particles (and consequently dissolved oxygen) between and around the gills, is at the origin of the kinematic switch. In other words, we propose to view the mayfly as a *stirring* rather than a *pumping* device as in earlier studies Sensenig *et al.* (2010); Abdelaziz *et al.* (2013). An effective transport/stirring mechanism may be seen as a way to provide a more efficient way in extracting oxygen from water, which is particularly relevant in anoxic waters as is the natural environment for the mayfly.

To study the transport performance we will utilize a dynamical systems strategy, which during the past two decades has provided new insights into a variety of fluid mechanics problems Grigoriev and Schuster (2011), most notably in small-scale fluid systems for which chaos theory has provided ways to create efficient and controllable micro-fluidic mixers Ottino (1990); Chabreyrie *et al.* (2008, 2011). To outline the basic principles of the approach let us start from an

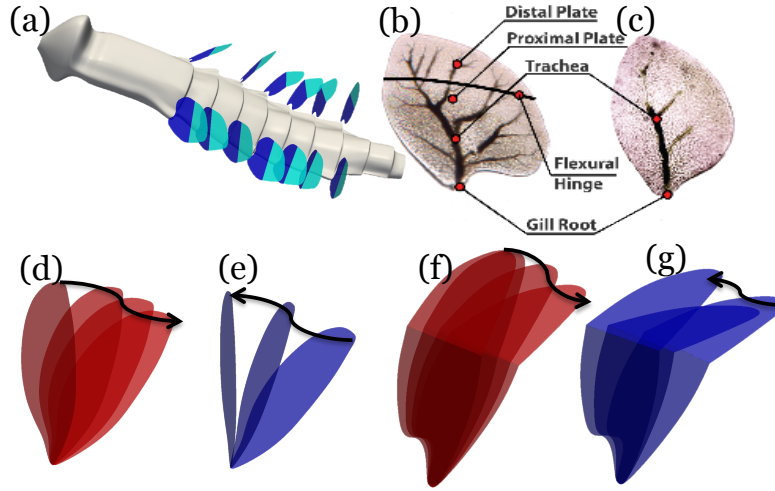


Figure 1: (a) In-silico model of mayfly nymph body with its seven pairs of gills. In-vivo gills: (b) mature mayfly; (c) young mayfly. In-silico rowing kinematics for a young mayfly: (d) retraction; (e) protraction. In-silico flapping kinematics for a mature mayfly: (f) retraction; (g) protraction.

Eulerian velocity field, \mathbf{V} , and consider the particle path equations,

$$\dot{\mathbf{X}}_{\mathbf{X}_0} = \mathbf{V}(\mathbf{X}_{\mathbf{X}_0}; t),$$

where $\mathbf{X}_{\mathbf{X}_0}$ represents the location of a Lagrangian particle at time, t , initially located at, $\mathbf{X}_0 = (x_0, y_0, z_0, t = 0)$. The solutions of this dynamical system or the flow ϕ^t , i.e. $\phi^t(\mathbf{X}_0) = \mathbf{X}_{\mathbf{X}_0}(t)$, give all the pathlines (or material lines) of the fluid flow generated by the velocity field, \mathbf{V} . In our case \mathbf{V} is obtained from the full Navier-Stokes simulations reported in Abdelaziz *et al.* (2013), where physiological characteristics (i.e. body shape, gills shape and kinematics) are carefully matched to replicate the conditions in the experiments with living mayfly nymphs reported in Sensenig *et al.* (2010). The in-silico mayfly used in these computations is shown in Fig. 1a, where one can observe how the gills are approximated with zero thickness, two-part, hinged plates. In the model a perfect bilateral symmetry is assumed for the mayfly body, gill shapes and motions.

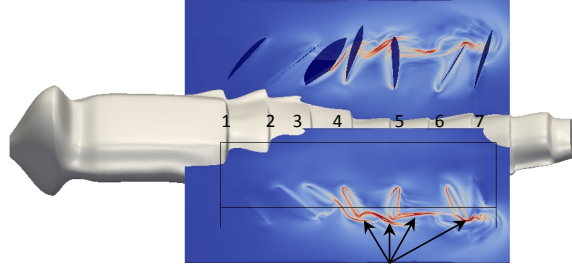
To better understand the physics that lead to the abrupt change in kinematics we will consider the following cases representing different stages of the mayfly's life: *i*) an early stage where the mayfly is around

1 – 2 days old; *ii*) a mature mayfly nymph, where the mayfly is around 40 days old. In the former case the gills resemble small plates with an average length of 0.3 mm that can be approximated by a rigid plate as shown in Fig. 1c-d. The Reynolds number is $Re = L^2 f \rho / \mu = 1.0$, where L , f , ρ and μ are the gill length, beating frequency, fluid density and viscosity, respectively. We should note that due to the lack of gill flexibility, at this Re the reciprocal flapping kinematics should result in negligible, on average, fluid transport. In the latter case, the gill size has increased drastically with an average length of 0.7 mm and the geometry has become more complex. In addition a flexural hinge develops as shown in Fig. 1b, f-g, and the gill is now approximated as a two-part hinged plate. The Reynolds number in this case is $Re = 21.6$.

First we will focus on identifying dynamically active barriers to transport, labeled as Lagrangian Coherent Structures (LCS) Haller (2000); Haller and Yuan (2000); Haller (2001a,b). These structures are now seen to be crucial in understanding transport phenomena in a variety of time-dependent systems ranging from large scale, e.g. oceanic Lekien *et al.* (1982); Rypina *et al.* (2010) or atmospheric Tang *et al.* (2010) flows, to small scale, e.g. hemodynamics Shadden *et al.* (2010); Arzani and Shadden (2012); Shadden and Hendabadi (2013); Duvernois *et al.* (2013) or swimming Dabiri *et al.* (2005); Wilson *et al.* (2009). These structures divide the fluid into dynamically distinct regions, revealing features hidden in the velocity field. In other words, these LCS act as attractive or repulsive barriers to transport for fluid particles. These attractive or repulsive LCS can be defined as the ridges of the Finite Time Lyapunov Exponent (FTLE) map calculated backward or forward in time. This map consists of associating an FTLE, \mathcal{L} , with an initial condition, \mathbf{X}_0 . The Lyapunov exponent can be seen as a measure of how two trajectories, starting initially close from each other, diverge. First, in order to compute the FTLE map, we consider the tangent flow

$$\dot{\mathbf{J}}^t = \nabla \mathbf{V} \mathbf{J}^t,$$

where \mathbf{J}^t and $\nabla \mathbf{V}$ are the Jacobian and matrix of variations, respectively. The initial condition is $\mathbf{J}^0 = \mathbf{I}$, where \mathbf{I} is the three-dimensional identity matrix. $\mathbf{J}^t(\mathbf{X}_0) = \partial \phi^t(\mathbf{X}_0) / \partial \mathbf{X}_0$ describes the deformation at time t of an infinitesimal sphere of neighboring initial conditions starting at \mathbf{X}_0 . Then, the FTLE map for a time, $t = \tau$, is



Self-contained LCS

Figure 2: FTLE field computed backward in time over five periods of gill oscillations for a young nymph ($Re = 1.0$) with rowing kinematics. For clarity we only plot two sections from the three-dimensional volume data: a horizontal section (bottom part), and an oblique section (top part). The attracting LCS is revealed by the ridges of the FTLE. Gills are shown in solid blue color.

computed as

$$\mathcal{L}(\mathbf{X}_0, \tau) = \frac{\ln |\gamma_{max}(\mathbf{X}_0)|}{|\tau|},$$

where γ_{max} is the largest eigenvalue (in norm) of J^τ . Finally, in order to reveal the LCS, ridges from the FTLE map, $\mathbf{X}_0 \rightarrow \mathcal{L}(\mathbf{X}_0, \tau)$, are extracted for a given time, τ . It is important to note that the LCS indicate a strong attractive or repulsive transport (i.e. local maximum in Lyapunov exponent map) on a thin restrained area (i.e. ridges). As the time of integration, τ , is increased this fine line or surface extends throughout the fluid space. Consequently, these LCS obtained by using the ridges of the FTLE map are localized where the most effective attractive and repulsive dynamics occur in the all fluid space. Since, in this work mayfly naids are seen as short time particle capturing/attracting systems, we will focus on capturing attractive LCS after a few oscillating periods of the gills.

Figures 2 and 3 display the FTLE field for: *i*) a young nymph at $Re = 1.0$ and, *ii*) a mature nymph at $Re = 21.6$. For both cases, the seven pairs of gills generate a complex three-dimensional unsteady velocity field, which in turn produces a very complex three-dimensional transport with embedded features. In order to clearly reveal these key features we plot two sections from the three-dimensional field: a

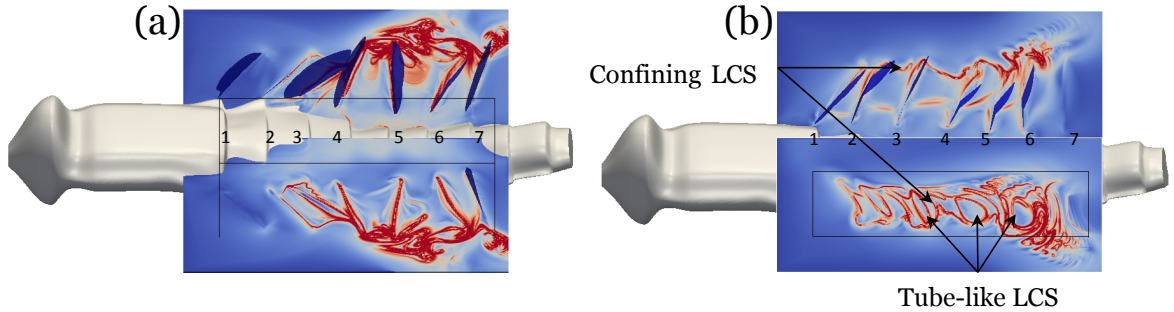


Figure 3: FTLE field computed backward in time over five periods of gill oscillations for mature nymph ($Re = 21.6$) with: (a) rowing kinematics; (b) flapping kinematics. For more details see caption of Fig. 2.

horizontal and an oblique section shown at the bottom and top parts of Figs 2 and 3 respectively. For each kinematic pattern these two sections are specifically selected to illustrate where the structures are the most relevant for transport.

i) In the case of a young nymph ($Re = 1.0$) with the rowing kinematic (the only gill motion possible), we see sharp ridges in the FTLE field corresponding to strong attractive LCS. From the horizontal and oblique sections of Fig. 2, we see that these LCS are mainly localized between gill pairs 3 – 6. Each gill generates its own self-contained attractive LCS going only along each respective gill (see horizontal section in Fig. 2) and then away from its tip with little transport generated in the inter-gill space (see oblique section in Fig. 2). Such a transport structure is a direct consequence of the fact that with rowing kinematics, each gill behaves as an independent (i.e. without interaction with its neighboring gills) single plate that mainly pushes fluid along and away from itself.

ii) For a mature nymph ($Re = 21.6$), both the rowing and flapping kinematics are possible. In the rowing case, although the LCS have been developed due to the increase of the Reynolds number, the transport structure is qualitatively the same as in the young nymph case. Each of the central gills 3 – 6 generates its own independent LCS that goes along each respective gill (see horizontal section in Fig. 3a)

and escape the gill area slightly above the mayfly body (see oblique section in Fig. 3a). The main difference with the young nymph is an extension of LCS from their gill tips to outside of the gill area (solid black lines in Fig. 3a). Such an extension of the LCS does not provide better attraction or capture for the gills. It simply provides a faster ejection of Lagrangian particles from the intra-gill area. In the flapping case, the transport structures change radically from the rowing cases. Fig. 3b clearly shows very neat ridges in the FTLE field, i.e. very strong LCS that display an intricate braiding of the transport structures, revealing two main features: From the top oblique section in Fig. 3b, one can observe that the gills generate a *confining LCS* structure. This confining LCS starts from gill pair 2 and encapsulates the gill area by joining the other gill tips and filling the inter-gill space. The other interesting feature is revealed from the horizontal section in Fig. 3b, where one can observe *tube-like LCS* between gill pairs 3 – 4, 4 – 5, 5 – 6 (see annotations in Fig. 3a). Such tube-like structures can be seen as *dynamical pockets* where Lagrangian particles are trapped. These two features indicate a transport mechanism of confinement of fluid particles, between and around the gills, which can be seen as a way to capture and extract more efficiently the dissolved oxygen in water.

From these qualitative observations, we can already understand the advantages of switching from rowing to flapping. When flapping kinematics is possible, i.e. gill flexibility and inertial effects are strong enough, elaborate transport structures are produced, which attract, stir and trap fluid particles between and around the gills. Although the qualitative results above point to the primary reason in the change of kinematics as the nymph grows, it is also important to provide quantitative measures of how well Lagrangian particles are stirred between and around the gills. Here we will quantify the degree of stirring as a function of spatial location by introducing the stirring index, M , through the box counting method Stremmer (2008). This technique offers the advantage of being relatively easy to implement, and computationally inexpensive. Let us follow N_p Lagrangian particles, and divide the domain enclosing the gills into, $N_x \times N_y \times N_z$ boxes (see black edges in Figs. 2, 3). At each time, t , the number of particles, n_i , inside each box, i , is computed and then the particle rate, r_i , is calculated as follows:

$$r_i = \frac{n_i}{n_p} \text{ if } n_i < n_p, \quad r_i = 1 \text{ if } n_i \geq n_p,$$

where n_p is the average number of Lagrangian particles, i.e. $n_p = N_p/(N_x N_y N_z)$. After computing the fraction of particles in each box and at each time, the time evolution of the stirring index, $M(t)$, is calculated by taking the average of $r(t)$ over all boxes:

$$M(t) = \frac{1}{N_x N_y N_z} \sum_{i=1}^{N_x N_y N_z} r_i(t), \quad \text{with } M(t) \in]0, 1[.$$

The case with the highest stirring index value corresponds to the case for which Lagrangian particles are spread widely and in the most uniform way inside the gill area. Such conditions enhance the spreading of dissolved oxygen in the water inside the gill area, and therefore enhance breathing performance. The stirring index, M , is shown in

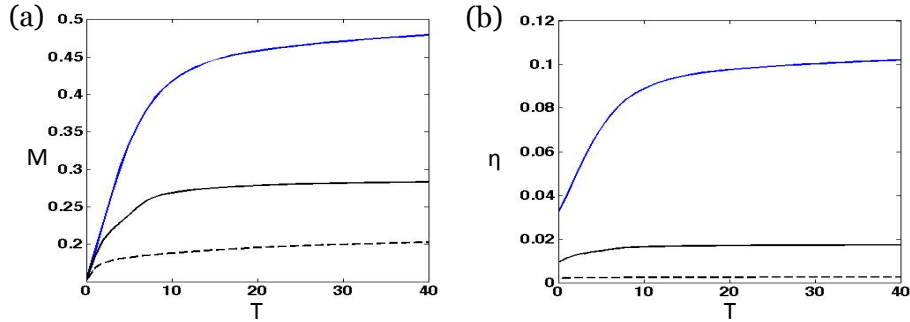


Figure 4: a) Stirring index and b) performance versus time computed over forty gill oscillation cycles, under $N_x \times N_y \times N_z = 45 \times 50 \times 150$, for $N_p = 10^8$ particles. Young nymph rowing kinematics (dashed line); mature nymph with rowing (solid black line) and flapping (solid blue line) kinematics.

Fig. 4a for the three cases considered, i.e. young nymph ($Re = 1.0$) with rowing kinematics, mature nymph ($Re = 21.6$) with both rowing and flapping kinematics. For the young nymph with rowing kinematics after a small increase, M ends up on a very small plateau around 0.2, indicating poor stirring. For the mature nymph with rowing kinematics we see that after a moderately fast increase phase, M reaches a pseudo plateau at medium height 0.28. For mature nymph with flapping kinematics, on the other hand, M shows a drastic increase in the stirring level all over the 40 periods considered. In particular, very steep growth is observed in less than 5 periods, where the value of M

reaches a high plateau of around 0.45. This is almost two times higher than the plateau attained by the rowing kinematics. This result reinforces the qualitative observations made earlier with the stransport structures: the switch to flapping kinematics enable the production of a transport mechanism that traps and stirs more than the crude and simple pumping transport generated by the rowing of the gills. The advantage of kinematics switching can even be more revealed by looking at the performance of the stirring. The stirring performance parameter, η , can be defined as the ratio between stirring index, M , and the average rate of work done by the gills over one period of oscillation:

$$\eta = M(t)/\overline{\dot{W}_{gills}},$$

where the rate of work \dot{W}_{gills} , is computed as:

$$\dot{W}_{gills} = \int_{gills} \mathbf{V} \boldsymbol{\tau} d\mathbf{A}, \quad \boldsymbol{\tau} = -P\mathbf{I} + \mu(\nabla\mathbf{V} + \nabla\mathbf{V}^T). \quad (1)$$

In the definition of the stress tensor, τ , in Eq. (1) above, P , \mathbf{I} and \mathbf{V} are the pressure, identity matrix and the velocity vector, respectively. $\overline{\dot{W}_{gills}}$ has been nondimensionalized by the gill length L , beating frequency f , fluid density ρ and viscosity μ . Fig. 4b displays the values of η over forty periods of gill oscillation for the three cases considered. For the young nymph η is extremely low $< .002$ showing very inefficient stirring transport. For the mature nymph with rowing kinematics, η is slightly higher but still represents a highly inefficient stirring system. As for the mature nymph with flapping kinematics η , increases excessively and reaches a plateau almost an order higher than in the rowing case at around $\eta \sim 0.1$.

In summary, this letter provides evidence on what causes the switch in gill kinematics as mayfly nymphs grow. Using a Lagrangian viewpoint, and looking at the mayfly nymph as a stirrer, we were able to show both qualitatively and quantitatively the advantages in switching from rowing to flapping as they grow. In particular, through the attracting LCS, we have qualitatively revealed that flapping kinematics generate a complex transport structure that attracts, stirs and confines around the gills, providing better access to the dissolved oxygen present in water. We reach the same conclusion by quantifying how well the fluid particles are stirred between the gills via the box counting method.

Overall for young nymphs, due to the lack of gill flexibility and inertial effects, rowing is the only way to create non-negligible fluid transport and generate a water current towards their body/gills. Consequently, through this simplistic transport structure, the gills can absorb some of the dissolved oxygen present in the water. In a mature nymph, on the other hand, the gills develop flexion lines, and due to their size inertial effects become important. In this case flapping kinematics generate a complex transport structure that greatly enhances oxygen extraction.

Support from the National Science Foundation, CBET-1067066, is gratefully acknowledged.

References

- Abdelaziz, K., E. Balaras, and K. Kiger (2013), *J. Fluid. Mech.* Submitted.
- Arzani, A., and S. C. Shadden (2012), *Phys. Fluids* **24** (8), 081901.
- Babák, E., and O. Foustka (1907), *Pflüger's Arch. f. Ges. Phys.* **119**, 530.
- Brennen, C., and H. Winet (1997), *Annu. Rev. Fluid Mech.* **9**, 339.
- Chabreyrie, R., C. Chandre, and N. Aubry (2011), *Phys. Fluids* **23** (7), 072002.
- Chabreyrie, R., D. Vainchtein, C. Chandre, P. Singh, and N. Aubry (2008), *Phys. Rev. E* **77**, 036314.
- Childress, S., and R. Dudley (2004), *J. Fluid Mech.* **498**, 257.
- Dabiri, J. O., S. P. Colin, J. H. Costello, and M. Gharib (2005), *J. Exp. Biol.* **208** (7), 1257.
- Daniel, T. L., C. Jordan, and D. Grunbaum (1992), “Hydromechanics of swimming,” Chap. *Mechanics of Animal Locomotion*, Alexander, R. M. ed. (Berlin: Springer-Verlag) pp. 17–49.
- Daniel, T. L., and P. W. Webb (1987), “Physical determinants of locomotion,” Chap. *Comparative physiology: life in water and on land*, Dejours, P. and Bolis, L. and Taylor, C. and Weibel, E. R. ed. (New York, NY: Liviana Press) pp. 343–369.

- Duvernois, V., A. L. Marsden, and S. C. Shadden (2013), *Int. J. Numer. Method. Biomed. Eng.* **29** (4), 445.
- Eastham, L. E. S. (1932), *Nature* **130**, 58.
- Eastham, L. E. S. (1934), *P. R. Soc. Lond. B-Conta.* **115** (791), 30.
- Eastham, L. E. S. (1936), *J. Exp. Biol.* **13**, 443.
- Eastham, L. E. S. (1937), *J. Exp. Biol.* **14**, 219.
- Fuiman, L. A., and R. S. Batty (1997), *J. Exp. Biol.* **200** (12), 1745.
- Gray, J., and G. J. Hancock (1955), *J. Exp. Biol.* **32**, 802.
- Grigoriev, R., and H. G. Schuster, Eds. (2011), *Transport and Mixing in Laminar Flows: From Microfluidics to Oceanic Currents* (Wiley-VCH).
- Haller, G. (2000), *Chaos* **10** (1), 99.
- Haller, G. (2001a), *Physica D* **149** (4), 248 .
- Haller, G. (2001b), *Phys. Fluids* **13** (11), 3365.
- Haller, G., and G. Yuan (2000), *Physica D* **147** (3-4), 352.
- Lekien, F., C. Coulliette, A. J. Mariano, E. H. Ryan, L. K. Shay, G. Haller, and J. E. Marsden (1982), *Physica D* **210**, 1.
- Lighthill, J. (1976), *SIAM Review* **18**, 161.
- Motani, R. (2002), *Nature* **415**, 309.
- Ottino, J. M. (1990), *Annu. Rev. Fluid Mech.* **22**, 207.
- Rypina, I. I., L. J. Pratt, J. Pullen, J. Levin, and A. L. Gordon (2010), *J. Phys. Oceanogr.* **40**, 1988.
- Sensenig, A. T., K. T. Kiger, and J. W. Shultz (2009), *Biol. J. Linn Soc.* **98** (3), 540.
- Sensenig, A. T., K. T. Kiger, and J. W. Shultz (2010), *J. Exp. Biol.* **213**, 3319.

- Shadden, S. C., M. Astorino, and J.-F. Gerbeau (2010), *Chaos* **20** (1), 017512.
- Shadden, S. C., and S. Hendabadi (2013), *Biomech. Model. Mechan.* **12** (3), 467.
- Spedding, G. R., M. Rosén, and A. Hedenström (2003), *J. Exp. Biol.* **206** (14), 2313.
- Strathmann, R. R. (1993), *Annu. Rev. Ecol. Syst.* **24**, 89.
- Stremmer, M. A. (2008), “Encyclopedia of microfluidics and nanofluidic,” Chap. Mixing measures, Li, D. ed. (Berlin: Springer-Verlag).
- Tang, W., P. W. Chan, and G. Haller (2010), *Chaos* **20** (1), 017502.
- Taylor, G. (1951), *Proc. R. Soc. Lond. A* **209** (1099), 447.
- Walker, J. A. (2002), *Integr. Comp. Biol.* **42** (2), 232.
- Webb, P. W., and D. Weihs (1986), *T. Am. Fish. Soc.* **115** (1), 115.
- Wigglesworth, V. B. (1931), *Biol. Rev.* **6** (2), 181.
- Wilson, M. M., J. Peng, J. O. Dabiri, and J. D. Eldredge (2009), *J. Phys.: Condens. Matter* **21** (20), 204105.